ELSEVIER

Journal of Structural Geology 26 (2004) 1293–1301

JOURNAL OF STRUCTURAL GEOLOGY

www.elsevier.com/locate/jsg

Orebody geometry in lode gold deposits from Zimbabwe: implications for fluid flow, deformation and mineralization

T.G. Blenkinsop

School of Earth Sciences, Economic Geology Research Unit, James Cook University, Townsville, Queensland 4811, Australia

Received 23 September 2002; received in revised form 24 January 2003; accepted 14 March 2003

Abstract

The geometry of some orebodies can be described simply and accurately by three orthogonal axes, $U \geq V \geq W$. The ratios between these axes can be expressed as a parameter $j = (U/V - 1)/(V/W - 1)$, and represented by a graph of U/V plotted against V/W, analogous to the treatment of strain ellipsoids. The orientations of orebodies can be plotted simply on projections using the UVW axes. Measurements of ore bodies from two examples of lode gold deposits from the Zimbabwe craton show that most of these orebodies are oblate. However, orebodies can have significant U/V ratios, implying a component of pipe-like fluid flow during mineralization. Pipe flow is demonstrated to be orders of magnitude more conductive than flow in planar veins and faults. There are significant variations in orebody geometry between deposits and within different sections of a single deposit. W values appear to be influenced by host rock: more permeable rocks have higher W. A negative trend of j value with orebody volume indicates that orebodies do not evolve in a self-similar way, but tend to more oblate shapes with increasing volume.

Keywords: Orebody; fluid flow; mineralization; gold; self-similar; Zimbabwe

1. Introduction

The geometry of a hydrothermal orebody depends on the interactions between fluid flow, host rock types and structures. There may be additional feedback between deformation, chemical reactions and mineralization for syntectonic orebodies. In homogeneous host rocks, the relation between orebody geometry, fluid flow and deformation may be relatively simple, and the geometry of the orebodies may therefore give insights into mineralising processes on scales of hundreds of metres. These scales are orders of magnitude larger than those accessible from laboratory measurements of permeability and structure, which commonly underpin conceptual models of fluid flow in deformation zones (e.g. Caine et al., 1996; Evans et al., 1997).

Orebodies can be classified into discordant and concordant bodies, and further into regular and irregular shapes (e.g. Evans, 1995). Regular orebodies are subdivided qualitatively into tabular and tubular shapes. Orebody geometry (shape and orientation) needs to be well understood and described quantitatively in order to be useful in investigations of fluid flow and mineralization, and to understand the structural controls on mineralization. The major aim of this paper is to propose a method for describing some orebody geometries simply and accurately, based on familiar concepts in structural geology. The method has direct applications to exploration, and it may be useful in fluid flow modelling and ore deposit studies. Two examples of epigenetic gold deposits in Zimbabwe (the Arcturus and Shamva deposits; Fig. 1) are used to illustrate the methods of describing orebody geometry. The results have some implications for fluid flow in mineralizing shear zones and the evolution of orebodies.

2. A simple method to describe orebody geometry

At some level of detail, all orebodies have complex geometries. One of the challenges of understanding a structurally-controlled orebody is to be able to describe the orebody simply enough to relate it to structures, yet in a quantitative way, that can allow comparison to be made between different deposits. A three-dimensional approach is necessary: in the general case, horizontal or vertical sections will be arbitrary planes through an orebody. Measurements made from sections, such as strike length, strike orientation (e.g. from level plans), or down-dip length and dip amount

E-mail address: thomas.blenkinsop@jcu.edu.au (T.G. Blenkinsop).

0191-8141/$ - see front matter © 2004 Elsevier Ltd. All rights reserved.
doi:10.1016/j.jsg.2003.11.010

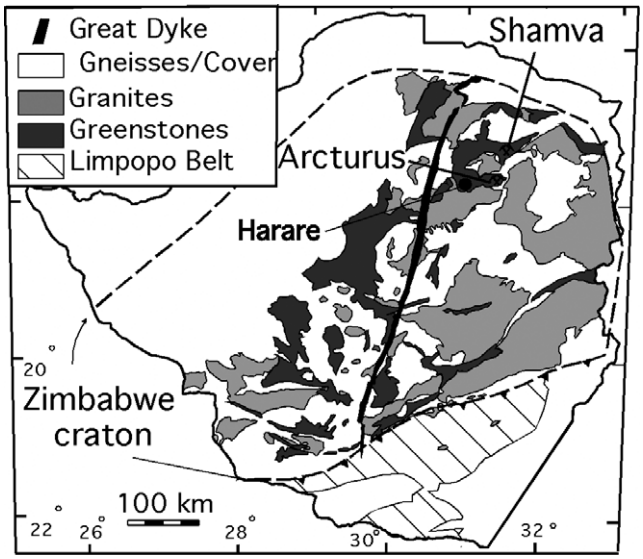

Fig. 1. Map showing the locations of Arcturus and Shamva mines.

(e.g. from vertical cross-sections) will be arbitrary sections through an orebody (see below), and therefore have little significance for characterising its true geometry.

A simple and accurate description of orebody geometries can potentially be made if three mutually perpendicular axes (maximum, intermediate and minimum) can be defined for the orebody (Fig. 2a). The geometrical description of an orebody could thus include measurements of the lengths of the three axes, and the orientations of two of them. It is useful in some circumstances to think of the ellipsoid that is defined by the three axes as an approximation to the shape of the orebody (Fig. 2b), although the definition and use of the three axes is not dependent on this approximation. The three axes of the orebody can be defined as $U \geq V \geq W$, and the orientations of the axes specified by the plunge and plunge bearing (trend) of the axes. The letters *UVW* have been chosen to avoid possible confusion with the axes of the strain ellipsoid $X \geq Y \geq Z$. Level plans or vertical cross-sections will not generally contain the axes of orebodies: this illustrates why measurements from these sections are inadequate to characterise these orebody dimensions and orientations (Fig. 2c).

The shape of the strain ellipsoid is commonly described by the *k*-parameter: $k = (X/Y - 1)/(Y/Z - 1)$ (e.g. Hobbs et al., 1976; Ramsay and Huber, 1987; Park, 1997). The orebody shape can also be characterised by a similar parameter $j = (U/V - 1)/(V/W - 1)$, which varies from ∞ for cigar-shaped (prolate) shapes to 0 for pancake-shaped (oblate) shapes. A useful graph to represent shapes can be constructed by plotting U/V vs. V/W (Fig. 3): for strain ellipsoids, this is known as the Flinn graph (Flinn, 1962). Here it will be referred to as the shape graph. Logarithmic axes are useful for data that have a large range of U/V and V/W ratios. The 'plane strain' line where $j = 1$ divides the plot into prolate and oblate fields and gives a ready and quantifiable visual indication of the difference between

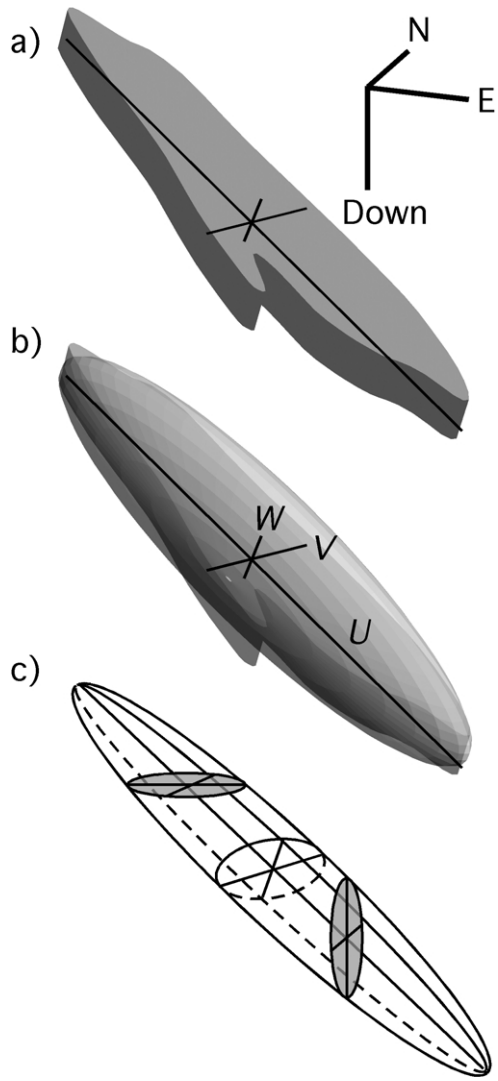

Fig. 2. (a) Schematic orebody with three axes defined. (b) The ellipsoid that is defined by the three axes can be considered as an approximation to the shape of the orebody. (c) Shaded ellipses show horizontal and vertical sections through the ellipsoid. The axes of these ellipses do not correspond to the orebody axes, and their planes do not correspond to the principal planes of the orebody ellipsoid.

tubular and tabular orebodies (e.g. Evans, 1995). The orientation of orebodies on a stereoplot can be represented by points corresponding to the axes of the orebodies and by great circles representing the *UV*, *VW*, or *UW* planes.

Advantages of this method are:

- It is simple
- Existing mine data will generally be adequate to allow measurements of the orebody axes to be made
- Comparisons between orebodies are facilitated by the systematic approach

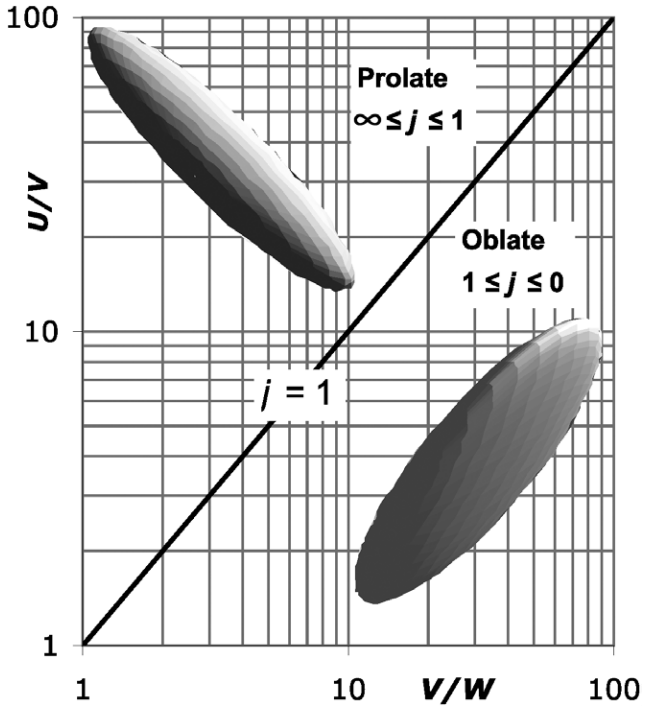

Fig. 3. The shape plot for orebody geometry.

Obvious possible problems with the approach may be:

- The orebody axes may be difficult to define, particularly where the shortest dimension is not perpendicular to the longest dimension
- Axes may be difficult to define for curved, folded and irregular bodies
- Faulted orebodies may not be adequately approximated as ellipsoids
- Orebodies with mixed characters e.g. veins with disseminated ore, may not be easily described by three axes

In addition to these obvious problems, it may be difficult to evaluate the significance of the orebody axes if there has been more than one episode of mineralization.

In practice, the identification of three axes in an orebody is almost certainly affected by some of the problems above. However, the task is facilitated by the natural geometry of many orebodies, which consist of sheet-like shapes. *W* is easily identified in orientation (perpendicular to the sheet) and in size (the orebody dimension perpendicular to the sheet is almost constant). *U* is usually easy to identify on a projection perpendicular to *W*, and *V* is taken as the perpendicular bisector of *U* in this plane. For orebodies with sub-horizontal *W*-axes, measurements can be made on longitudinal projections (this was the case for the Arcturus example of this study). It is easy to make the measurements interactively on a computer wireframe model of the orebody (as done for the Shamva example here). An alternative approach to direct measurement would be to use an ellipsoid fitting routine. Ellipsoids could be chosen to totally enclose the orebody, or to have the same volume as the orebody. Directional variography could also be used to assist with definition of the axes.

It is difficult to estimate the error involved in these measurements, which varies with each axis and with each orebody. By far the greatest source of error will be the uncertainty in the demarcation of the orebody, generally made from extrapolation of drilling results. Allowing for an error of 10 m in the *U* and *V* directions will potentially introduce an error of 10 and 20% in these two directions, based on the average values of this study. The value of *W* is usually much better constrained because drilling is commonly in this direction, and *W* may be contained within a single drive. The results reported here should not therefore be regarded as more accurate than these values, which are nevertheless sufficient for the general level of interpretations made in this study.

3. Open, closed and uncertain orebodies

The original geometry of orebodies that intersect the surface or have not been proven at depth is unknown and these types of orebody offer much less information about mineralizing processes than fully-demarcated orebodies. On the other hand, they are of major interest for mine development. For both reasons, they need to be carefully identified, and they are distinguished as open here. When using older mine records, it may be unclear whether orebodies are open or not. Therefore a three-fold classification has been used in this study (Fig. 4):

- Open orebodies (part or all of the orebody boundary is undefined)
- Closed orebodies (the boundary of the orebody is fully defined)

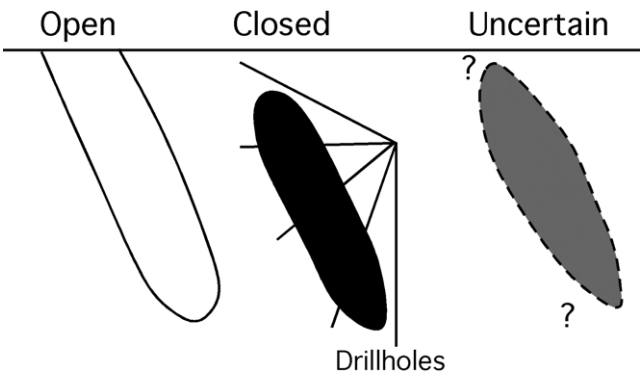

Fig. 4. Three types of orebodies. Open orebodies have part or all of their boundaries undefined, such as the example on the left, which is intersected by the surface. Closed orebodies have all boundaries fully defined, for example by assay results from drilling. For uncertain orebodies, the nature of part or all of their boundaries is not clear.

- Uncertain orebodies (the nature of part or all of the boundaries is unknown)

4. Geological background: Arcturus and Shamva gold deposits

4.1. Arcturus deposit

The Arcturus deposit lies 30 km E of Harare in the Harare–Shamva–Bindura greenstone belt (Fig. 1), hosted mainly by metabasalts of the Arcturus formation (Baldock, 1991) with minor felsites and meta-ultramafites. Hydrothermal muscovite from a mineralization-hosting shear zone in the deposit yielded an Ar–Ar age of 2688 ± 15 Ma (Mutemeri, 2001), which is consistent with regional considerations that suggest a late Archean age for the Arcturus Formation and therefore the minimum age of the gold mineralization. The orebodies consist of disseminated pyrrhotite, arsenopyrite, and pyrite within an alteration assemblage of biotite–actinolite–quartz–epidote–fuchsite–feldpsar (from metabasalts) and sericite–quartz–feldspar (from felsite). P–T conditions of mineralization were 100–240 MPa and from 200–520 °C (Mutemeri, 2001).

The Arcturus deposit consists of four major sections (from W–E: Arcturus, Venus, Gladstone and Ceylon; Fig. 5) over an E–W strike distance of 8 km. Strong S–L schistosities within shear zones associated with the mineralization underground and on the surface indicate that the four sections are contained within a major shear zone about 1 km wide, known as the Arcturus shear zone (Fig. 5). Gold mineralization is clearly syntectonic since auriferous sulphides of a common generation are both deformed in the shear zone and overprint the shear fabrics (Mutemeri, 2001). The planar fabrics dip steeply N–NE, and biotite and actinolite mineral lineations plunge steeply to the NE and N within the shear zone (Fig. 5), but its kinematics are not obvious since no asymmetry can be seen in sections parallel to the mineral stretching lineation. The shear zone may have a major component of pure shear (Blenkinsop, 2001).

4.2. Shamva deposit

The Shamva deposit also lies in the Harare–Bindura–Shamva greenstone belt, 90 km to the NE of Harare (Fig. 1). Host rocks to the deposit belong to the Shamvaian supergroup, and consist of argillites, greywackes, conglomerates, pyroclastic sediments (crystal tuffs) and plagioclase porphyries (Foster et al., 1986). The intrusion age of the porphyries is constrained by a U–Pb zircon TIMS age of 2672 ± 12 Ma (Jelsma et al., 1996), and these are probably the feeders for the pyroclastic components of the host rocks. This is therefore a minimum age for mineralization, which fits into the pattern of late Archean mineralization in the greenstone belt. Orebodies are dominated by pyrite and carbonate, within an alteration assemblage of biotite–tourmaline–sulphide–oxide–carbonate–quartz (± graphite). P–T conditions during mineralization are estimated at 100–300 MPa and 250–450 °C (Jelsma et al., 1998).

Shamva deposit lies within the NE-striking Shamva shear zone, which is defined by subsidiary shear and fault zones over a minimum strike distance of 1.5 km and a width of 150–300 m (Fig. 6; Jelsma et al., 1998). Within the shear zone, NW, W and SW striking, sub-vertical faults carry subhorizontal slickenfibre lineations defined by chlorite, quartz and carbonates, and steps that indicate sinistral strike slip movement with a minor reverse component. Sinistral strike-slip movement is also indicated by S–C fabrics in decimetre-wide shear zones. Orebodies formed along these fault zones, as indicated by localization of mineralization and alteration along and between fault planes (Fig. 6).

5. Results

Measurements of closed orebodies are summarised in Table 1, and all the results are plotted on shape graphs in Fig. 7 with stereoplots in Fig. 8.

5.1. Arcturus deposit

There is considerable variation in orebody geometry within the Arcturus deposit, but all measurements plot

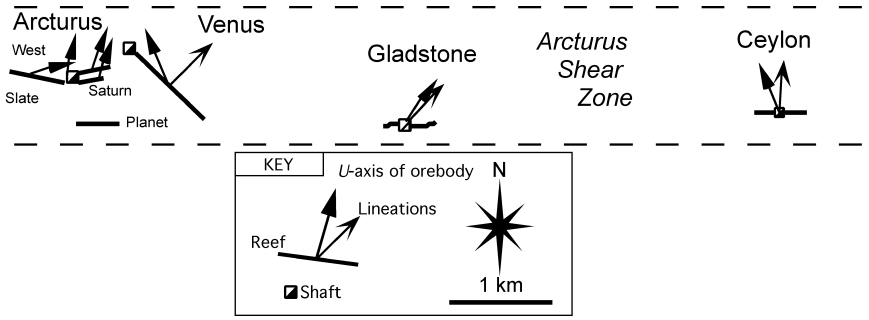

Fig. 5. Locations of the four sections of the Arcturus deposit, the Arcturus shear zone, and fabric elements in the deposits.

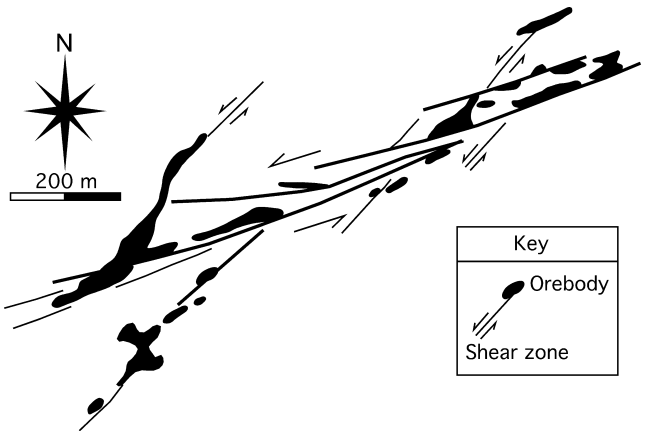

Fig. 6. Map of the Shamva deposit showing major shear zones and orebodies (after Jelsma et al., 1998).

below the $j = 1$ line in the oblate field (Table 1; Fig. 7a). The four closed measurements from the Arcturus section, and all the measurements from the Gladstone and Ceylon sections, plot well within the oblate field (Fig. 7a), but the closed measurement from the Venus section has a higher j value (0.822), approaching the prolate field. As a whole, the measurements from this section have higher U/V ratios than the other sections of the mine. The orebodies at Arcturus plunge steeply (Fig. 8a) to the N–NE.

5.2. Shamva deposit

There is also considerable spread in the orebody geometry at Shamva (Fig. 7b). The average of the 31 closed orebodies plots low within the oblate field (Table 1; $j = 0.23$). The data spread along a trend with a negative slope in the shape plot. The U-axes of the orebodies plunge steeply to the SW–NE (Fig. 8b), while the W-axes are sub-horizontal and trend perpendicular to the dominant NE–ENE strikes of the Shamva shear zone.

6. Discussion

6.1. The effect of lithology

Although orebodies at Shamva and Arcturus both have low j values, there is a very clear distinction of orebody geometry on the shape plot, in which all the Arcturus orebodies have larger V/W ratios than any of the Shamva orebodies (Fig. 7). An obvious reason is the narrow widths of the orebodies at Arcturus (the average W dimension of closed orebodies at Arcturus is 1.9 m compared with 9 m at Shamva). This in turn may relate to more confined fluid flow through the massive, relatively impermeable metabasalt host rocks at Arcturus, compared with the more permeable metasedimentary host rocks of the Shamva deposit. The validity of this explanation is supported by evidence of low W dimensions (2 m) in the Muriel mine, Zimbabwe craton, which is also hosted by metabasalts and has similar characteristics to the Arcturus deposit (Blenkinsop, 2002).

6.2. Differentiation of orebody geometry within the same structure

Different parts of the Arcturus shear zone have different orebody shapes (Fig. 7a) and orientations (Fig. 8a). The single closed measurement from the Venus section has a much higher U/V value than other parts of the mine, and orebodies in this section plunge to the NW compared with the N–NE plunge of orebodies in the other sections. There is a significant difference in geometry between the Venus part of the Arcturus shear zone and the other parts: the Venus section of the Arcturus shear zones strikes SE–ESE compared with the general E strike of the shear zone. This change in orientation within the Venus section is clearly an original feature of the Arcturus shear zone, since folding would produce orebody orientations that plunged to the E. There is also an important variation in orebody orientation between the Gladstone and Ceylon sections: orebodies in the former plunge NNW, compared with NNE–ENE plunges in the latter.

It is highly significant for mine development that orebody shape and orientations change with the host shear

Table 1
Means and standard deviations (SD) of dimensions and j values for closed orebodies. SDs only reported for four or more measurements. N = number of measurements

Deposit	U		V		W		j		N
	Mean	SD	Mean	SD	Mean	SD	Mean	SD	
Arcturus									
Arcturus	410	253	94	50	1.5		0.107	0.132	4
Venus	600		38		2		0.822	0.000	1
Gladstone	202		32		1.5		0.285	0.014	2
Shamva	108	55	64	35	8.6	4.1	0.230	0.036	31

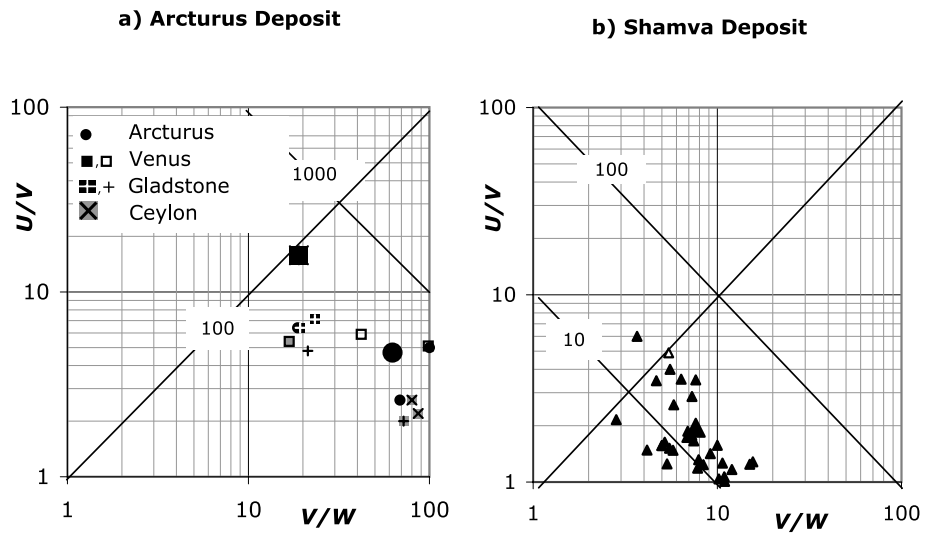

Fig. 7. Shape plot for orebodies at (a) Arcturus and (b) Shamva. Diagonal lines with numbers represent lines of constant *U*/*W* ratio, indicated by the numbers. The diagonal line in the opposite direction is the line separating oblate from prolate orebody shapes. Note that this diagram includes the open and uncertain ore bodies, unlike Table 1. Symbols with black background are closed orebodies (Table 1); grey background signifies uncertain orebodies and white background are open orebodies. Large symbols are average values, given for the closed orebodies only.

zone. The significance for understanding the processes of orebody formation is less clear, particularly because of the paucity of closed orebodies in the Venus section.

6.3. Effect of kinematics and deformation zone architecture

A similarity between the Arcturus and Shamva deposits is the sub-vertical orientation of the *U*-axes of the orebodies, despite differences in the kinematics of their hosting shear zones. The *U*-axes of the orebodies are orientated generally down-dip within their hosting shear zones. The kinematics of the Arcturus shear zone are probably dominated by pure shear, which produced a strong sub-vertical mineral stretching lineation (Blenkinsop, 2001), while lineations in the Shamva shear zone are sub-horizontal and the shear zone has simple shear, strike-slip kinematics (Jelsma et al., 1998). These characteristics may indicate that kinematics of shear zones are less important than vertical hydraulic gradients in determining fluid flow and individual orebody geometry. In both cases, intersecting faults or shear zones may have been the dominant influence on permeability.

Intersections appear to determine the gross geometry of the orebodies, while shear directions may control high-grade ore shoots.

6.4. Planar vs linear orebodies

A striking aspect of the data (Fig. 7) is the tendency for orebodies to have geometries with considerable *U*/*V* ratios. These elongations cannot be attributed to deformation of the orebodies at Shamva, since they are perpendicular to the shear direction. It is also unlikely that the elongations reflect deformation of the orebodies at Arcturus, since some mineralization is undeformed (cf. Mutemeri, 2001). The

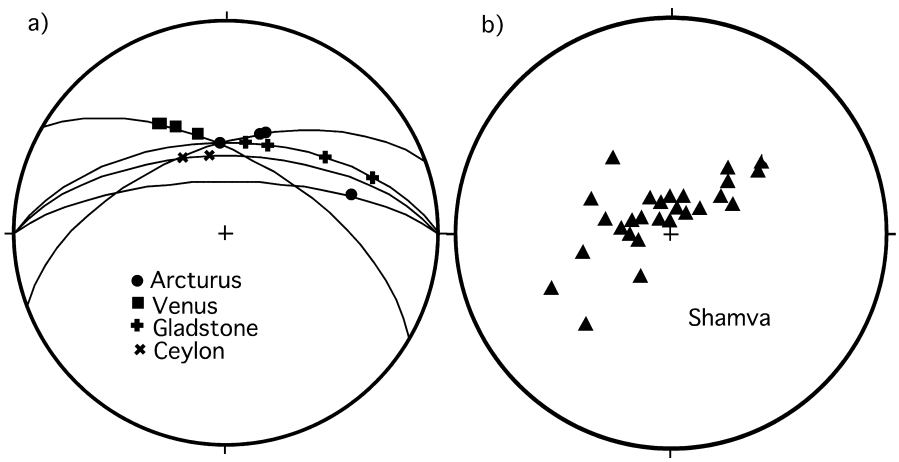

Fig. 8. (a) Stereoplots of *U*-axes to orebodies, *UV* planes of orebodies and structural data for Arcturus. (b) Stereoplots of *U*-axes to orebodies for Shamva (*UV* planes were not accurately measured). All projections are lower hemisphere, equal area.

geometry of these syntectonic orebodies thus indicates a component of pipe-like fluid flow.

The conductivity of fluid flow through pipes can be compared with fractures (e.g. Sanderson and Zhang, 1999). If Qf is the conductivity through a fracture of aperture a and length L, and Qp conductivity through a pipe of radius r, Δp is the pressure gradient and μ is the viscosity, then:

$$Qf = \frac{a^3 L \Delta p}{12\mu}$$

$$Qp = \frac{\pi r^4 \Delta p}{8\mu}$$

$$\frac{Qp}{Qf} = \frac{\pi r^4 \Delta p}{8\mu} \times \frac{12\mu}{a^3 L \Delta p}$$

$$= \frac{1.5\pi r^4}{a^3 L}$$

$$= \frac{1.5L}{\pi a}$$

since

$$r = \left(\frac{aL}{\pi}\right)^{1/2}$$

for the same surface area. Thus the relative conductivity of pipe flow over fracture flow with the same cross-sectional areas increases with the length/aperture (L/a) ratio of the fracture.

Table 2 presents measurements and estimates of the L/a ratio of veins. Johnston and McCaffrey (1996) concluded that L of natural fractures was related to a by a power law with an exponent of 0.6–1. Simplifying this relationship by taking the exponent to be unity will give minimum values of L/a, which are 20–2000 from their results (Table 1). Johnston and McCaffrey (1996) also show that vein aspect ratios increase as veins lengthen beyond a critical value, which corresponds to a change in growth mechanism. Other measurements of L/a in Table 1 range from 28 to 10000.

Two important questions about how the measured L/a ratios of veins apply to actual conditions of fluid flow concern the thickness of the vein that has been filled at any time, and the width that may be open to fluid flow, possibly supported by supra-lithostatic pore fluid pressures. The questions can in part be addressed theoretically. The relation predicted by linear elastic fracture mechanics for L/a is:

$$\frac{L}{a} = \frac{\pi\mu/(1-\nu)}{4(P-S)}$$

where μ is the shear modulus, ν is Poisson's ratio, P is the fluid pressure and S the crack-normal stress (e.g. Pollard, 1987). $P-S$ is known as the driving stress. A limiting value for the driving stress might be considered to be the tensile strength of rock, which ranges from 1 to 40 MPa (e.g. Blenkinsop, 2000). ν is typically 0.25, and μ may range from 1 to 100 GPa (Jaeger and Cook, 1979). This gives a range of L/a from 25 to 10^5 using the extreme values, or from 1000 to 2500 making the assumption that tensile strength and μ are correlated. Since these ranges encompass all the observed values, it is reasonable to suggest that the in-situ measurements of aspect ratios are not radically different from those during fluid flow. These measurements imply that pipe-like flow may be between 10 and 5000 times more conductive than the equivalent fracture flow.

The relationship between L and a for faults has been the subject of considerable debate in the literature (e.g. Hull, 1988, 1989; Blenkinsop, 1989; Evans, 1990). Although it appears that no simple relationship exists, the data presented in Evans (1990) indicate a general minimum value for L/a of 10 and maximum values in excess of 1000, suggesting that pipe conductivity is between 5 and 500 times greater than fracture conductivity for faults. The formation of orebodies with significant U/V ratios by pipe-like flow is thus associated with a dramatic increase in conductivity compared with the formation of more tabular orebodies by fracture flow.

6.5. Self-similar vs. self-affine evolution of orebody geometry

One of the most striking features about Fig. 7 is the spread of j values along lines of negative gradients on the shape plots. It is reasonable to assume that data sets from individual deposits may contain orebodies in various stages of growth; thus the spread in data indicates a change in j value with evolution of the orebody. Orebodies do not appear to grow in a self-similar manner.

To test this idea further, j values have been plotted as a function of the approximate orebody geometry given by the volume of the ellipsoid defined by U, V, and W for the closed bodies only (Fig. 9). There is a general negative trend

Table 2
Length (L) and aperture (a) relationships and measurements from natural fractures and veins, and from linear elastic fracture mechanics (LEFM)

Host rock	$L-a$ relationship	L/a	Reference
Quartzite, calcarenite. calcsilicates, sandstones, marbles, granites	Power Law	20–2000	Johnston and McCaffrey (1996)
Basalts	Linear	400	Gudmundsson et al. (2001)
Limestone	Log normal	1000–10000	Gillespie et al. (2001)
Turbidites	Power law	Averages 28–67	Stowell et al. (1999)
LEFM	Linear	25–100000	Pollard (1987)

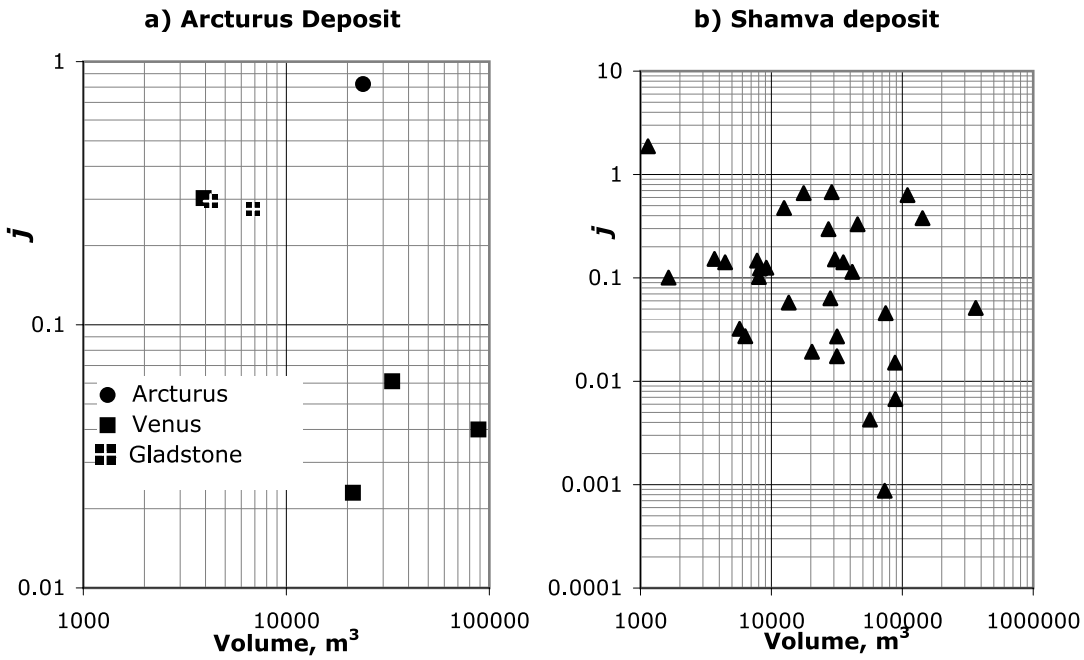

Fig. 9. j vs. orebody/shear zone ellipsoid volume: (a) Arcturus and (b) Shamva. Only closed orebodies/shear zones are shown; symbols as in Fig. 7.

between j value and orebody size, although there are very few data from Shamva. This suggests the interesting result that some orebodies may change from less to more oblate shapes as they grow, as shown schematically in Fig. 10. Orebody evolution may not be not self-similar but instead may be self-affine, following a law such as $j \sim \text{volume}^{-d}$ where d is a constant.

7. Conclusions

The geometry of some relatively simple orebodies can be characterised by defining three mutually perpendicular axes ($U \geq V \geq W$), and the orebody geometry can be specified by the lengths and orientations of these axes. As might be anticipated for syntectonic hydrothermal orebodies in planar deformation zones, the dominant shapes of the orebodies studied here are oblate.

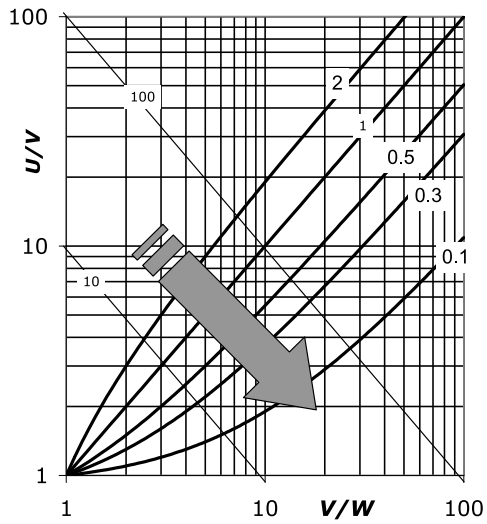

Fig. 10. Schematic evolution of orebodies on a shape plot (large arrow), showing schematically how orebodies evolve towards lower j-values. Numbered lines are loci of constant j-values: self-similar orebody evolution would track along these lines.

Host rock type (specifically permeability) has a fundamental influence on orebody geometry through its effect on W-dimensions. Smaller W-dimensions are associated with less permeable rocks. The shapes and orientations of orebodies may change within a single host structure, with major potential implications for mine development.

Intersecting elements of deformation zones provide permeability guides that lead to pipe-like fluid flow, which is associated with orders of magnitude greater conductivity than fractures of equivalent cross-section. This is manifested in significant U/V ratios of orebodies.

One of the most interesting results of the geometric analysis is that orebody geometry changes as a function of size from less to more oblate. This indicates that orebody evolution may not be not self-similar.

Acknowledgements

The support of Independence Gold Mining Zimbabwe is gratefully acknowledged, including particularly the chief geologists at Arcturus and Shamva, Kosmas Chenjerai and Oliver Mapeto. Simon Dominy is thanked for discussions, and Susan Vearncombe and Michael Meyer for useful reviews.

References

Baldock, J.W., 1991. The geology of the Harare Greenstone belt and surrounding granitic terrain. Bulletin 94, Zimbabwe Geological Survey.

Blenkinsop, T.G., 1989. Thickness-displacement relationships for deformation zones: discussion. Journal of Structural Geology 11, 1051–1052.

Blenkinsop, T.G., 2000. Deformation Microstructures in Minerals and Rocks. Kluwer Academic Publishers, Dordrecht.

Blenkinsop, T.G., 2001. Deformation and Fluid Flow in Transpression: Insights from Hydrothermal Ore Body Geometry. Abstracts, Deformation Mechanisms, Rheology and Tectonics Meeting, Utrecht, Netherlands.

Blenkinsop, T.G., 2002. Ore deposit geometry in deformation-hosted gold deposits. In: McLellan, J., Brown, M. (Eds.), Deformation, Fluid Flow and Mineralisation (Rick Sibson Symposium), EGRU Contribution 60, James Cook University, pp. 4–10.

Caine, J.S., Evans, J.P., Foster, C.B., 1996. Fault zone architecture and permeability structure. Geology 24, 1025–1028.

Evans, A.M., 1995. Introduction to Mineral Exploration. Blackwell Science Limited, Oxford.

Evans, J.P., 1990. Thickness-displacement relationships for fault zones. Journal of Structural Geology 12, 1061–1066.

Evans, J.P., Forster, C.B., Goddard, J.V., 1997. Permeability of fault related-rocks, and implications for hydraulic structure of fault zones. Journal of Structural Geology 19, 1393–1404.

Flinn, D., 1962. On folding during three-dimensional progressive deformation. Quarterly Journal of the Geological Society of London 118, 385–428.

Foster, R.P., Furber, F.M.W., Gilligan, J.M., Green, D., 1986. Shamva Gold Mine, Zimbabwe: a product of calcalkaline-linked exhalative, volcaniclastic and epiclastic sedimentation in the late Archean. In: Keppie, J.D., Boyle, R.W., Haynes, S.J. (Eds.), Turbidite-hosted Gold Deposits. Geological Society of Canada Special Paper 32, pp. 41–66.

Gillespie, P.A., Walsh, J.J., Watterson, J.J., Bonson, C.G., Manzocchi, T., 2001. Scaling relationships of joint and vein arrays from The Burren, Co. Clare, Ireland. Journal of Structural Geology 23, 183–201.

Gudmundsson, A., Berg, S.S., Lyslo, K.B., Skurtveit, E., 2001. Fracture networks and fluid transport in active fault zones. Journal of Structural Geology 23, 343–353.

Hobbs, B.E., Means, W.D., Williams, P.F., 1976. An Outline of Structural Geology. John Wiley and Sons, New York.

Hull, J., 1988. Thickness-displacement relationships for deformation zones. Journal of Structural Geology 10, 431–435.

Hull, J., 1989. Thickness-displacement relationships for deformation zones—reply. Journal of Structural Geology 11, 1053–1054.

Jaeger, J.C., Cook, N.G.W., 1979. Fundamentals of Rock Mechanics, 3rd ed, Chapman and Hall, London.

Jelsma, H.A., Vinyu, M.L., Valbracht, P.J., Davies, G.R., Wijbrans, J.R., Verdurmen, E.A.T., 1996. Constraints on Archean crustal evolution of the Zimbabwe Craton: a U–Pb zircon, Sm–Nd and Pb–Pb whole-rock isotope study. Contributions to Mineralogy and Petrology 124, 55–70.

Jelsma, H.A., Huizenga, J.M., Touret, J.L.R., 1998. Fluids and epigenetic gold mineralization at Shamva Mine, Zimbabwe: a combined structural and fluid inclusion study. Journal of African Earth Sciences 27, 55–70.

Johnston, J.D., McCaffrey, K.J.W., 1996. Fractal geometries of vein systems and the variation of scaling relationships with mechanism. Journal of Structural Geology 18, 349–358.

Mutemeri, N., 2001. Fluids and gold mineralization at Arcturus mine, Zimbabwe. PhD Thesis, University of Zimbabwe.

Park, R.G., 1997. An Outline of Structural Geology, 3rd ed, Chapman and Hall, London.

Pollard, D.D., 1987. Elementary fracture mechanics applied to the structural interpretation of dykes. In: Halls, H.C., Fahrig, W.F. (Eds.), Mafic Dyke Swarms, Geological Association of Canada Special Paper 34, pp. 5–24.

Ramsay, J.G., Huber, M.I., 1987. The Techniques of Modern Structural Geology, Vol. 1. Academic Press, London.

Sanderson, D.J., Zhang, X., 1999. Critical stress localization of flow associated with deformation of well-fractured rock masses, with implications for mineral deposits. In: McCaffrey, K.J.W., Lonergan, L., Wilkinson, J.J. (Eds.), Fractures, Fluid Flow and mineralization. Geological Society Special Publication 155, pp. 69–81.

Stowell, J.W.F., Watson, A.P., Hudson, N.F.C., 1999. Geometry and population systematics of a quartz vein set, Holy island, Anglesey, North Wales. In: McCaffrey, K.J.W., Lonergan, L., Wilkinson, J.J. (Eds.), Fractures, Fluid flow and Mineralization. Geological Society Special Publication 155, pp. 17–33.